Enhanced Long-Term Stability of a Photosensitizer with a Hydroxamic Acid Anchor in Dye-Sensitized Photocatalytic Hydrogen Generation

Giorgia Salerno+,[a, b] Bianca Cecconi+,[a, c] Ottavia Bettucci,[a] Matteo Monai,[d, e] Lorenzo Zani,[c] Daniele Franchi,[c] Massimo Calamante,[c, f] Alessandro Mordini,*[c, f] Tiziano Montini,*[d] Paolo Fornasiero,[d] Norberto Manfredi,[a] and Alessandro Abbotto*[a]

Climate change mitigation on a global scale will only be possible through the achievement of ambitious decarbonisation goals, requiring an energy transition that involves switching from fossil fuels to clean fuels such as hydrogen. The photocatalytic approach is one of the most studied methods for directly converting sunlight into hydrogen. In this work, we present the synthesis, characterization, and application of the **PTZ1-HA** dye, which was obtained by replacing the terminal conventional carboxylic anchoring moieties of a previously studied phenothiazine-based dye (**PTZ1**) with hydroxamic acid functionalities. The photoinduced performance of the two dyes as photosensitizers was compared in both

dye-sensitized solar cells and dye-sensitized photocatalytic systems. **PTZ1-HA**-sensitized photocatalysts showed improved stability in hydrogen generation due to the introduction of the hydroxamic acid as an alternative anchor group, which was shown to slow down hydrolysis in aqueous media. Even though the light harvesting ability of **PTZ1-HA** was lower than that of **PTZ1**, the higher stability of **PTZ1-HA**-sensitized devices allowed for improved photocatalytic generation of H_2 over prolonged periods. The superior long-term efficiency of the hydroxamic acid based dye is important in view of potential practical applications.

Introduction

Fossil fuels have been playing a fundamental role in our society since the inception of the industrial revolution, providing the energy required to improve the standards of living of a large share of the world population. Despite such important function, however, fossil

fuels also present major issues.[1] The main limitations include environmental pollution, non-renewability, and uneven geographical dislocation.[2] For all these reasons, an ecological transition is now needed by replacing fossil fuels with renewable energy sources.[3] In this scenario, a way to satisfy the need for solar energy storage is the direct conversion of solar radiation (also known as

[a] Dr. G. Salerno,+ Dr. B. Cecconi,+ Dr. O. Bettucci, Prof. N. Manfredi, Prof. A. Abbotto
Department of Materials Science and
Milano-Bicocca Solar Energy
Research Center (MIB-SOLAR)
University of Milano–Bicocca
Via Cozzi 55, 20125 Milano (Italy)
E-mail: alessandro.abbotto@unimib.it
Homepage: https://en.unimib.it/alessandro-abbotto

[b] Dr. G. Salerno+
Department of Information and Electrical
Engineering and Applied Mathematics (DIEM)
Invariante 12/B, Via Giovanni Paolo II, 132
84084 Fisciano (SA) (Italy)

[c] Dr. B. Cecconi,+ Dr. L. Zani, Dr. D. Franchi, Dr. M. Calamante, Dr. A. Mordini
Institute of Chemistry of Organometallic
Compounds (CNR-ICCOM)
Via Madonna del Piano 10
50019 Sesto Fiorentino (Italy)
E-mail: alessandro.mordini@unifi.it

[d] Dr. M. Monai, Prof. T. Montini, Prof. P. Fornasiero
Department of Chemical and Pharmaceutical Sciences
INSTM Trieste Research Unit and
ICCOM-CNR Trieste Research Unit
University of Trieste
Via L. Giorgieri 1
34127 Trieste (Italy)
E-mail: tmontini@units.it

Homepage: http://meeresearch.weebly.com/montini.html

[e] Dr. M. Monai
Inorganic Chemistry and Catalysis Group
Institute for Sustainable
and Circular Chemistry and Debye Institute for
Nanomaterials Science
Utrecht University
3584 CG Utrecht (The Netherlands)

[f] Dr. M. Calamante, Dr. A. Mordini
Department of Chemistry "U. Schiff"
University of Florence
Via della Lastruccia 13
50019 Sesto Fiorentino (Italy)
Homepage: http://www.iccom.cnr.it/it/single-profile-iccom/?uid=139

[+] These authors contributed equally to the work

🖳 Supporting information for this article is available on the WWW under https://doi.org/10.1002/ejoc.202300924

EurJOC
European Journal of Organic Chemistry

Research Article
doi.org/10.1002/ejoc.202300924

Chemistry Europe
European Chemical Societies Publishing

artificial photosynthesis) into valuable chemicals and fuels through water splitting or carbon dioxide reduction.[4] The photocatalytic approach is one of the most investigated methods to convert sunlight into chemicals.[5]

In a photocatalytic process, a semiconductor (SC, *e.g.*, TiO_2) absorbs light and transfers the excited electron from its conduction band (CB) to a co-catalyst (*e.g.*, Pt) where the production of solar chemicals takes place.[6] Critical requirements for an efficient SC are absorption of a large portion of the visible light, proper alignment of its energy levels with those of the co-catalyst, and stability under working conditions.[7] While the last two conditions are easily satisfied by many SCs, light harvesting is always a tough compromise.[8] The most convenient way to extend the absorption spectrum of a SC to the visible portion of the solar radiation is its sensitization by a molecular dye using an organometallic or a metal-free organic sensitizer.[9]

The energetic requirements in dye-sensitized photocatalysis (DSPC) are similar to those of dye-sensitized solar cells (DSSCs).[9c,10] Indeed, many DSSC sensitizers can also be successfully used in DSPC.[9a,d] In the last years, many researchers have investigated several types of sensitizers that improve photocatalytic performances through molecular engineering, which optimizes light harvesting, stability, and surface interaction.[9b,11] The anchoring/acceptor group is strongly involved in both the injection of electrons and the stability of the dye on the semiconductor surface, thus playing a central and strategic role in the whole process.[12]

Cyanoacrylic acid has been so far the most common choice as anchoring group in many DSSC and DSPC sensitizers.[13] The superior electron-withdrawing ability, due to the presence of the strong cyano acceptor group, and the good anchoring stability of the carboxylic acid functionality, favoured its predominant use compared to other functional group with similar characteristics.[14] Indeed, this is the case when working in an organic environment, such as that typically found in a DSSC (e.g., when using an acetonitrile/valeronitrile mixture as the electrolyte solvent). However, cyanoacrylic acids suffer from some limitations, especially related to long-term stability issues of the ester-like bonding between the dye and the TiO_2 surface, in the presence of an aqueous medium, such as that found in aqueous DSSCs or required in DSPC water splitting.[15] To solve this issue, alternative anchoring units capable of forming robust linkages to the TiO_2 surface have been proposed: an overview of the literature on organometallic complexes and their *ad hoc* modification for use in aqueous medium shows that phosphonic acids are usually the preferred option for replacing carboxylic moieties.[16] However, efficient electronic communication is often limited by this group because of tetrahedral phosphorous geometry.[17] Accordingly, asymmetric anchors have been proposed where the electronic communication is ensured by a carboxylic functionality whereas the strong binding character is played by phosphonic acid.[18]

Stability is an important parameter to optimize in order to ensure the practical application of the devices.[19] There are two aspects in durability: stability of the dyes upon irradiation (photostability) and against hydrolysis of the connection between dye and SC. The first requirement can be fulfilled through proper modification of the spacer unit, thanks to the peculiar behaviour of thiophene derivatives.[20] Careful attention should now be focussed on the development of a more stable covalent grafting of the dye on the TiO_2 surface.

Hydroxamic acids have been selected as promising candidates as they allow efficient electronic communication with the SC like that of carboxylic acids.[21] The strength of the covalent bond with TiO_2 surface has been calculated by both mixed quantum-classical molecular dynamics,[22] and DFT to be at least one third more stable upon hydrolysis reaction in a water environment.[23] This is mainly due to the fact that hydroxamic acids can form a strong bridging complex with coordinatively unsaturated Ti atoms on the TiO_2 surface. Furthermore, when a nitrogen centre of the hydroxamic acid functionality is involved in the covalent binding to the SC surface, a highly stable and more hydrolysis resistant amide-type bond is formed in contrast with the weaker ester bond.

Despite these encouraging premises, so far very few examples have been reported in the literature concerning the exploitation of the hydroxamic acid anchoring group in DSSC dyes,[24] To our knowledge, no previous use of the hydroxamic acid anchor group for DSPC hydrogen generation has been reported, despite the more stringent requirements in terms of anchoring stability due to the presence of an aqueous medium. The ideal anchoring-acceptor candidate to be investigated would therefore consist in a cyano-hydroxamic acid, where both the robust electron-withdrawing capacity of the nitrile group and the high stability against hydrolysis in water of the hydroxamic acid have been suitably combined. To investigate this hypothesis, we have chosen phenothiazine-based sensitizers, which have resulted in improved long-term H_2 photo generation and stability under irradiation Accordingly, in this work **PTZ1**, a reference phenothiazine-based sensitizer carrying two terminal conventional cyano-carboxylic acid anchors, that some of us have previously investigated as an efficient dye for DSPC hydrogen generation,[9a,25] has been modified to investigate the effect of replacing the original anchoring functionalities with terminal cyano-hydroxamic acids. The new dye **PTZ1-HA** (Figure 1) has been synthesized and investigated, in comparison with the reference PTZ1, as a sensitizer in DSSCs and DSPCs for hydrogen evolution.[26] A comparative stability study has been also carried out, highlighting the superior performances of the new dye compared to the reference.

Results and Discussion

Among the various synthetic approaches available to convert a carboxylic into a hydroxamic acid[27] we have chosen to treat carboxylic precursor **PTZ1** with 4-(4,6-dimethoxy-1,3,5-triazin-2-yl)-4-methylmorpholinium-chloride (DMTMM), a commonly
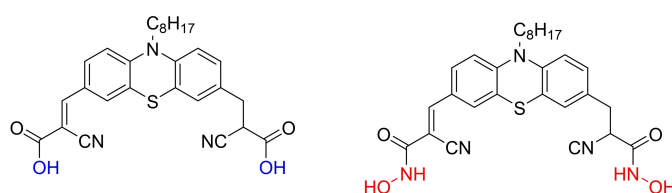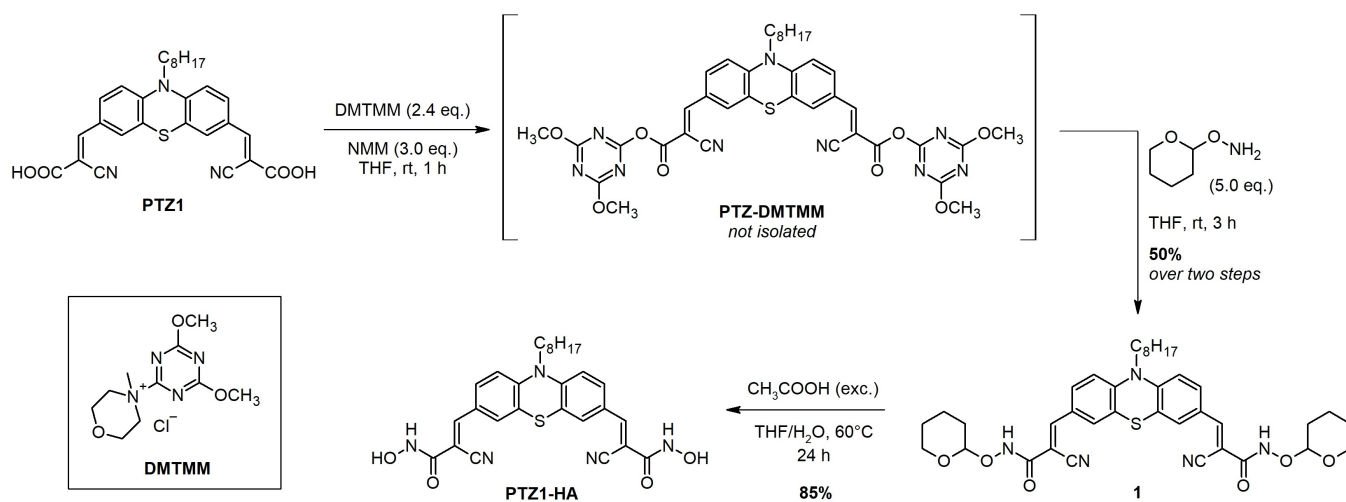

Figure 1. Structures of the two dyes investigated in this work: the new hydroxamic acid derivative **PTZ1-HA** and the reference **PTZ1**.

EurJOC
European Journal of Organic Chemistry

Research Article
doi.org/10.1002/ejoc.202300924

Chemistry Europe
European Chemical Societies Publishing

Scheme 1. Synthetic route for **PTZ1-HA**.

used activating agent for peptide couplings,[28] in the presence of *N*-methylmorpholine (NMM) as a base.

As previously reported in the literature,[29] this procedure affords an activated 2-acyloxy-1,3,5-triazine intermediate (Scheme 1), which can then easily undergo a reaction with a nitrogen nucleophile such as hydroxylamine or a derivate thereof.[30] As commonly carried out in peptide synthesis, this intermediate was not isolated and purified, but its alleged formation was monitored by TLC and further supported by the darkening of the reaction mixture (from red to dark red, due to the bathochromic effect induced by the presence of the strongly conjugated and electron-withdrawing triazine units). The hydroxamic moiety was then introduced as a THP (tetrahydropyran)-protected form by *in situ* addition of *O*-(tetrahydro-2*H*-pyran-2-yl)hydroxylamine (THP-O-NH$_2$) to the reaction mixture. Such protection allowed to conduct a proper purification through column chromatography, otherwise hampered by the presence of free hydroxamic acid groups. Finally, the desired product was obtained by cleavage of the THP group in the presence of an excess of acetic acid in a THF/H$_2$O mixture. **PTZ1-HA** was isolated by filtration and purified just by washing with different organic solvents, to avoid hydrolysis to the starting carboxylic acid. The overall reaction sequence is illustrated in Scheme 1.

Optical and Electrochemical Characterization

Optical characterization of **PTZ1-HA** has been carried out in comparison with **PTZ1**. The UV-Vis absorption spectra of both compounds are depicted in Figure 2. Both dyes present an intense intramolecular charge-transfer (ICT) band in the 400–550 nm region according to the literature.[9a,25a] The shape of the ICT absorption band in the Vis region is broader for **PTZ1-HA**. Both dyes present a main transition around 450–460 nm (with a slight blue shift of 12 nm for **PTZ1-HA**) and then a second transition at ca. 400 nm which appears as a shoulder in **PTZ1** and is more visible in **PTZ1-HA**. The molar extinction coefficient
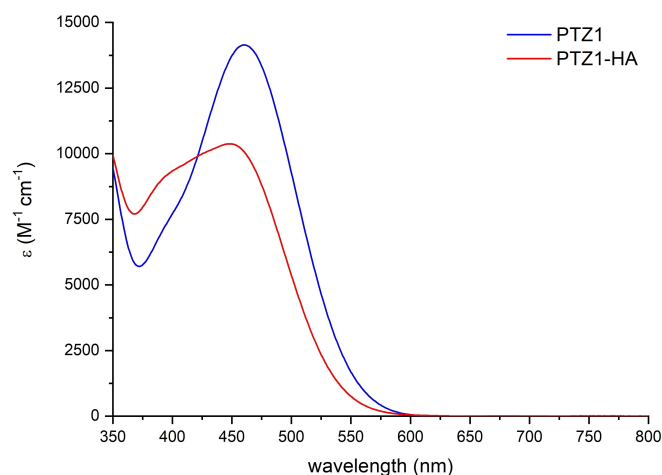

Figure 2. UV/Vis absorption spectra of **PTZ1** and **PTZ1-HA** in THF solution (10^{-5} M).

of the main Vis peak is lower in **PTZ1-HA**. Overall, the optical properties of the two dyes are similar, with a somewhat lower intensity of the hydroxamic acid derivative, that should be considered when studying their photocatalytic behaviour. Tauc plots have been used to evaluate E_{gap}^{opt}. All the optical parameters are listed in Table 1.[25c,31]

A 10^{-3} M solution of **PTZ1-HA** in DMSO was used for the electrochemical characterization in the presence of N(nBu)$_4$ClO$_4$ (0.1 M) as the supporting electrolyte. The cyclic voltammetry (CV) study of the new dye (Figure 3, dashed line) showed a quasi-reversible behaviour at oxidative potentials (potential > 0 V *vs.* Fc/Fc$^+$) and few irreversible reduction waves at the lowest potentials (potential < -1.0 V). Upon this behaviour, differential pulse voltammetry (DPV) was preferred to determine the oxidation (E^{ox}) and reduction (E^{red}) potentials (Figure 3, solid line) so to calculate the HOMO and LUMO energy levels, as listed in Table 1.

The measured oxidation potential and the calculated energy of the HOMO level for **PTZ1-HA** are consistent with those

EurJOC
European Journal of Organic Chemistry

Research Article
doi.org/10.1002/ejoc.202300924

Chemistry
Europe
European Chemical
Societies Publishing

Table 1. Optical[a] and electrochemical[b] parameters for **PTZ1** and **PTZ1**-**HA**.

Dye	λ_{max} (nm)	ε (M^{-1} cm^{-1})	λ_{onset} (nm)	$E_{gap}^{opt[c]}$ (eV)	E^{ox}(V) ± 5 mV	HOMO (eV) ± 50 meV	LUMO (eV) ± 50 meV
PTZ1[d]	460	13700 ± 300	590	2.10	0.39	-5.62	-3.52
PTZ1-**HA**	448	10500 ± 450	579	2.14	0.52	-5.81	-3.67[e]

[a] 10^{-5} M solution in THF; [b] All potentials are reported vs. Fc/Fc$^+$, and the HOMO and LUMO energies are calculated from the electrochemical data based on the assumption that the Fc/Fc$^+$ redox couple is 5.29 eV relative to a vacuum, using a potential value of 4.6 ± 0.2 eV for NHE vs vacuum[34] and 0.69 eV for Fc/Fc$^+$ vs NHE; [c] Measured by Tauc plots; [d] Values from ref [25]; [e] Calculated from electrochemical HOMO energies and optical bandgap.
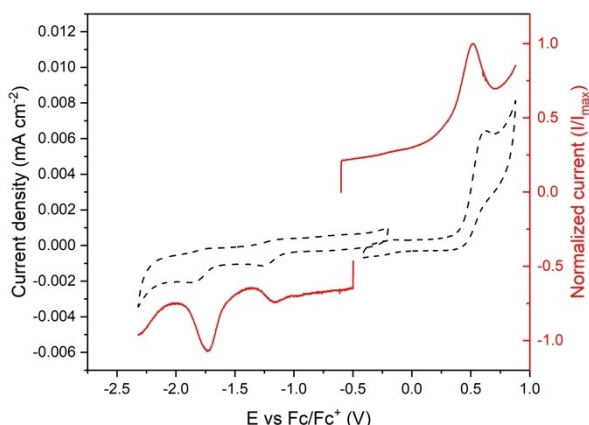

Figure 3. CV (dashed line) and DPV (solid line) of **PTZ1**-**HA** (10^{-3} M solution in DMSO with 0.1 M N(nBu)$_4$ClO$_4$).
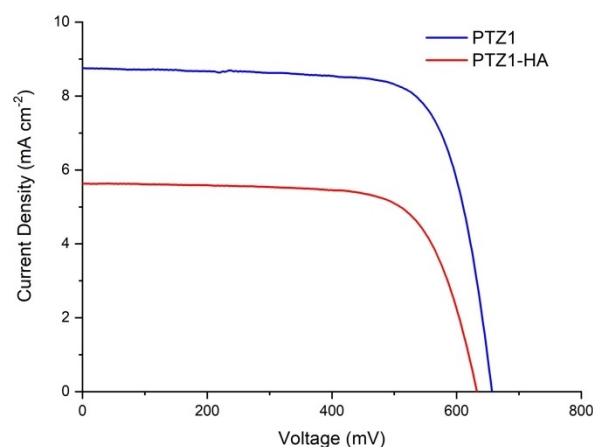

Figure 4. J/V curves for **PTZ1** and **PTZ1**-**HA** sensitized solar cells under full AM 1.5 G solar intensity with a 0.38 cm^2 black metal mask on top.

previously reported for **PTZ1**,[25c] as expected since the phenothiazine donor core is the same for both molecules. In contrast, a different behaviour was expected upon reduction, which may be affected by the presence of different acceptor-anchoring units in the two dyes. The CV plot shows two reduction waves as previously observed for **PTZ1**, which are related to the processes of reductive chemisorption of the acid protons on the electrode surface and injection of electrons into the LUMO orbital.[32] For this reason, the value of the LUMO was evaluated from the corresponding HOMO energy and the optical bandgap. The calculated LUMO level appears adequate for allowing efficient electron injection into the CB of the TiO$_2$-based catalyst.[33]

Photovoltaic investigation

DSSC devices have been investigated in order to compare the photovoltaic activities of **PTZ1** and **PTZ1**-**HA**. Since very few reports of dyes bearing hydroxamic acids are present in the DSSC literature,[21,24b,35] a careful screening of the photovoltaic performances is thus appropriate.[24c] Furthermore, comparing the relative efficiencies provided by the two sensitizers in DSSC and in the DSPC hydrogen production system could also prove useful to assess the influence exerted by the different media (organic solvent in DSSC and water in DSPC) in the two devices. Figure 4 shows the current density/voltage plots of the corresponding DSSCs. The recorded power conversion effi-

ciency (PCE) of the cell containing the hydroxamic acid dye is almost half that of the carboxylic acid counterpart. This is mostly due to a significantly lower photocurrent density (J_{sc}) in **PTZ1**-**HA** sensitized cells, whereas fill factors (FF) and photovoltages (V_{oc}) are comparable. The main photovoltaic characteristics are listed in Table 2.

The lower photo-current could be ascribed to a reduced dye loading or to a less efficient electron injection from the excited state of the dye to the CB of TiO$_2$. It should be also considered that optical characterization has outlined a lower light harvesting efficiency for **PTZ1**-**HA** that could be responsible for the lower PCE.

Table 2. Photovoltaic characteristics of **PTZ1** and **PTZ1**-**HA** sensitized DSSCs.[a]

Dye	J_{sc} (mA cm^{-2})	V_{oc} (mV)	FF (%)	PCE (%)
PTZ1	8.76 (11.1)	656 (667)	74 (74)	4.3 (5.5)
PTZ1-**HA**	5.01 (5.63)	627 (618)	66 (65)	2.1 (2.3)

[a] Conditions: Dye solution in EtOH (2×10^{-4} M) with 1:1 chenodeoxycholic acid; electrolyte Z960 (Solaronix, 1.0 M dimethyl imidazolium iodide, 0.03 M I$_2$, 0.05 M LiI, 0.1 M guanidinium thiocyanate and 0.5 M 4-t-butilpiridine in acetonitrile/valeronitrile 85/15, single TiO$_2$ layer (10 μm); surface area 0.20 cm^2. Values in brackets are referred to measurements without mask.

EurJOC
European Journal of Organic Chemistry

Research Article
doi.org/10.1002/ejoc.202300924

**Chemistry
Europe**
European Chemical
Societies Publishing

Anchoring stability testing

We have investigated stability towards desorption as a relevant tool to assess the comparative strength of the bond formed between the dyes **PTZ1** and **PTZ1-HA** and the SC surface.[36] The experiment is performed by accelerating the desorption process of sensitized TiO_2 films (analogous to those used for DSSC fabrication) in an alkaline solution of 0.1 M KOH in EtOH/H_2O 15:1.[37] Comparative stability towards desorption was determined by measuring the residual amount of anchored dye on the TiO_2 surface by means of UV/Vis spectroscopy of solid transparent films in transmittance mode. Due to the roughness and relative inhomogeneity of the film surface, spectra were recorded at different points of it and average and standard deviation values were calculated. The relative residual absorbance values are illustrated in Figure 5.

The **PTZ1-HA** sensitized TiO_2 film showed a higher stability towards accelerated desorption, which is ascribed to the presence of the hydroxamic acid in place of the carboxylic acid anchoring functionality. After 20 min of accelerated desorption, the residual amount of **PTZ1-HA** anchored dye (as estimated by the relative absorbance) is almost twice as large as that of **PTZ1**. Moreover, the desorption process is levelled off in the case of **PTZ1-HA** after 20 min, whereas the residual absorbance of the anchored dye keeps decreasing for **PTZ1**.

Photocatalytic hydrogen production

Photocatalytic hydrogen production experiments were carried out using a composite Pt/TiO_2 catalyst, prepared by irradiating a suspension of Degussa P25 TiO_2 nanoparticles in water/EtOH in the presence of a suitable amount of $Pt(NO_3)_3$ precursor with a 450 W high pressure Hg lamp. The UV irradiation induces the reduction of Pt^{2+} ions and allows the deposition of Pt(0) nanoparticles on the surface of the TiO_2. The obtained material was then sensitized with both dyes, resulting in a dye loading of 10 $\mu mol\,g^{-1}$, accordingly to previous studies performed under

Figure 6. H_2 production rate measured using the **DYE**@TiO_2/Pt photocatalysts in hydrogen production experiments from TEOA 10 v/v% solution at pH = 7.0 under irradiation with visible light ($\lambda > 420$ nm).

optimised conditions.[25b] The photocatalytic H_2 production was performed using a dispersion of the obtained composite **DYE**@TiO_2/Pt catalyst in an aqueous solution of triethanolamine (TEOA) as sacrificial agent at pH = 7.0 under irradiation with visible light ($\lambda > 420$ nm) for 2 h. The obtained photocatalytic hydrogen production rates are presented in Figure 6 while the overall H_2 productivity are reported in Figure S1 and Table 3 along with the other appropriate figures of merit.[38]

Figure 6 shows that H_2 production rates sharply increased in the initial 2 hours of irradiation while, for longer periods, a progressive deactivation was observed with a different extent depending on the employed dye. This behaviour is in agreement with the previous results obtained with the **PTZ1** dye.[25c] Despite a comparable overall H_2 productivity over the 22 h of irradiation, **PTZ1** possesses better performance in the initial period while **PTZ1-HA** demonstrated a lesser extent in deactivation. As a result, **PTZ1** showed the highest maximum H_2 production rate after 2 hours of irradiation while **PTZ1-HA** showed higher values after the initial 8 hours of irradiation. Consequently, Light-to-Fuel Efficiency (LFE) is higher in the initial period for **PTZ1**@TiO_2/Pt (see LFE2 values in Table 3) while it becomes higher for **PTZ1-HA**@TiO_2/Pt for longer irradiation times (see LFE22 values in Table 3).
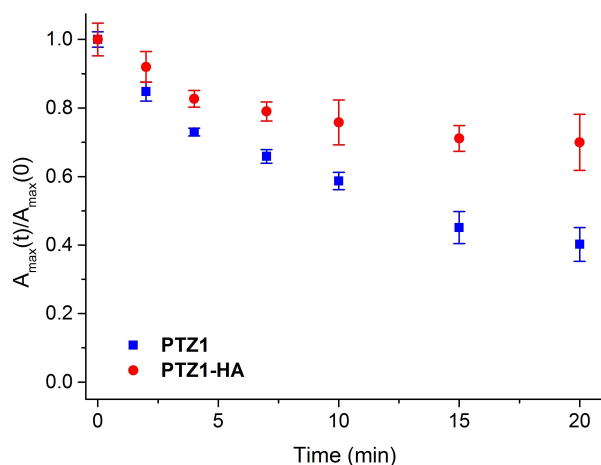

Figure 5. Relative residual absorbance values of **PTZ1**- (blue squares) and **PTZ1-HA**-sensitized (red circles) TiO_2 films upon accelerated desorption in an alkaline solution of 0.1 M KOH in EtOH/H_2O 15:1.
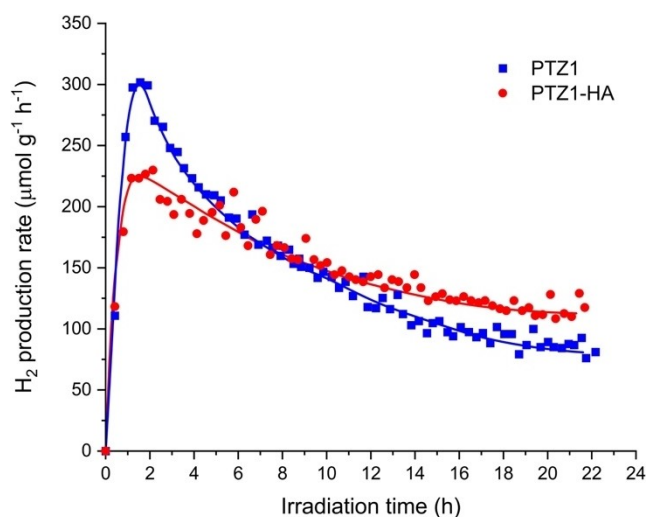
Table 3. Photocatalytic performances of the **DYE**@TiO_2/Pt catalysts in H_2 production from TEOA 10 v/v% solution at pH = 7.0 under irradiation with visible light ($\lambda > 420$ nm).

Dye	H_2 amount[a] [$\mu mol\,H_2\,g^{-1}$]	TON[b]	LFE2[c]	LFE22[d]
PTZ1	3224	644	0.134%	0.038%
PTZ1-HA	3302	660	0.102%	0.053%

[a] Overall H_2 amount produced after 22 h of irradiation. [b] TON = (2×H_2 amount)/(dye loading). [c] Light-to-fuel efficiency calculated after 2 h of irradiation. [d] Light-to-fuel efficiency calculated after 22 h of irradiation.

RIGHTS LINK

EurJOC
European Journal of Organic Chemistry

Research Article
doi.org/10.1002/ejoc.202300924

Chemistry
Europe
European Chemical
Societies Publishing

The overall H_2 productivity using the two composite photocatalysts are continuously increasing with irradiation time but showing slightly different trends (Figure S1). As a result, the TON calculated after 22 h of irradiation are very similar (Table 3). It is worth noticing that the overall H_2 productivity does not appear to be particularly affected by the weaker light-harvesting ability of the hydroxamic functionalized **PTZ1-HA** dye. Indeed, only after 19 h, the yield of H_2 provided by the **PTZ1-HA**@TiO$_2$/Pt photocatalyst even slightly surpassed that of **PTZ1**@TiO$_2$/Pt.

The data reported highlights that the stability of the hydroxamic derivative plays a crucial role when operating in water. In contrast with DSSCs where the dye-sensitized photoanode is in contact with an organic environment, in the aqueous medium of the H_2 production experiment the greater stability of the dye-TiO$_2$ bond via the hydroxamic acid functionality of **PTZ1-HA** compensates for its shortcomings in terms of optical properties. The obtained results clearly indicate a higher stability of the photocatalyst when **PTZ1-HA** is used as a dye. Such improved stability is most likely associated to the lower tendency of **PTZ1-HA** to desorb from the TiO$_2$ surface with respect to **PTZ1**. The stronger bound to TiO$_2$ surface could increase the probability of electron transfer from the excited dye to the CB of the semiconductor, reducing the self-degradation of the excited dye by intramolecular decay mechanisms and finally the loss of active sensitizer. As a result, the higher stability of the **PTZ1-HA** TiO$_2$ film limited the efficiency loss during the entire experiment, allowing to achieve a higher H_2 production rate compared to **PTZ1** at the end of the run.

Conclusions

We have synthesized and characterized a novel phenothiazine-based sensitizer (**PTZ1-HA**) for application in photocatalytic hydrogen production experiments. The new sensitizer carries a hydroxamic acid anchoring group, which was introduced in place of the conventional carboxylic acid moiety in order to improve the stability in the typical aqueous environment of the photocatalytic device. The new dye has been fully characterized in its structural and optical properties and then tested in DSSCs to evaluate its current generation capability in comparison with the reference dye **PTZ1** containing the carboxylic anchoring group. In solar cells using a mixture of organic solvents as electrolyte medium, the use of the new hydroxamic acid dye resulted in lower PCE values compared to the carboxylic acid analogue, probably due to its reduced light harvesting properties. In contrast, when working in the aqueous environment of the hydrogen photocatalytic production, the superior stability of the hydroxamic anchoring group versus the corresponding carboxylic acid, as ascertained by accelerated desorption tests in an alkaline aqueous solution, allowed to achieve similar and, for longer times, even improved H_2 production efficiencies. This behaviour is particularly evident when hydrogen generation rates are recorded: indeed, in spite of a lower value in the first hours, likely due to an intrinsic lower efficiency associated to

weaker optical properties, an increased performance has been recorded in the long run, with the **PTZ1-HA** sensitized photocatalyst becoming more efficient than that based on **PTZ1** after the first 8 hours. This result is remarkable if we consider that long-term efficiency is more important, in view of practical applications, than a performance peak only in the first hours.

This work highlights how a proper design of an efficient dye for sensitized photoactivated devices should not only consider the improvement of the intrinsic properties related to the photoactivated process, such as for example the light collection and the charge transfer efficiency, but also the specific environment in which the device will operate, taking into account the possibility of fruitful application in industrial or commercial operating environments in the long term.

Experimental Section

General information: NMR spectra have been recorded either with a Bruker AMX-500 spectrometer operating at 500.13 MHz (^{1}H) and 125.77 MHz (^{13}C), a Varian Gemini 200 spectrometer operating at 200 MHz (^{1}H) and 50.4 MHz (^{13}C), and a Varian Mercury 400 spectrometer operating at 400 MHZ (1H) and 100.8 MHz (^{13}C). Chemical shift values are expressed in ppm on the δ scale and referred to the residual solvent peaks (CDCl$_3$, δ 7.26 ppm for ^{1}H and δ 77.16 ppm for ^{13}C; DMSO-$d6$, δ 2.50 ppm for ^{1}H and 39.51 ppm for ^{13}C; THF-$d8$ δ 1.72 and 3.58 ppm for ^{1}H, δ 67.21 and 25.31 ppm for ^{13}C). Coupling constants (J) are expressed in Hz, while the used abbreviations are: s (singlet), d (doublet), dd (doublet of doublets), t (triplet), td (triplet of doublets), and m (multiplet). Multiplets are indicated as chemical shift intervals. ESI-MS analyses have been performed with a Thermo Scientific LCQ-FLEET instrument with infusion technique. Absorption spectra were recorded with a V-570 Jasco spectrophotometer and a Varian Cary 4000 spectrophotometer. Reactions performed under inert atmosphere were done in flame- or oven-dried glassware and a nitrogen atmosphere was generated with Schlenk technique.[39] All reagents were obtained from commercial suppliers at the highest purity grade and used without further purification. Anhydrous solvents were purchased from Sigma-Aldrich and used without further purification. Extracts were dried with Na$_2$SO$_4$ and filtered before removal of the solvent by evaporation. **PTZ1** was synthesized according to the literature.[25c] FTO-coated glass plates (2.2 mm thick; sheet resistance ~7 ohm per square; Solaronix), Dyesol 18NR-AO active opaque TiO$_2$ blend of active 20 nm anatase particles and up to 450 nm anatase scatter particles, and N719 (Sigma-Aldrich) have been purchased from commercial suppliers. UV-O$_3$ treatment was performed using Novascan PSD Pro Series-Digital UV Ozone System. The thickness of the layers was measured by means of a VEECO Dektak 8 Stylus Profiler.

Fabrication of the DSSCs

DSSCs have been prepared adapting a procedure reported in literature.[40] To avoid metal contamination all labware were treated with EtOH and 10% HCl prior to use. Plastic spatulas and tweezers have been used throughout the procedure. FTO glass plates were cleaned in a detergent solution for 15 min using an ultrasonic bath, rinsed with pure water and EtOH. After treatment in a UV-O$_3$ system for 18 min, the FTO plates were treated with a freshly prepared 40 mM aqueous solution of TiCl$_4$ for 30 min at 70°C and then rinsed with water and EtOH. An opaque active layer of 0.20 cm^2 was screen-printed using Dyesol 18NR-AO active opaque TiO$_2$ paste. The coated films were thermally treated at 125°C for 6 min, 325°C

for 10 min, 450 °C for 15 min, and 500 °C for 15 min. The heating ramp rate was 5–10 °C/min. The sintered layer was treated again with 40 mM aqueous $TiCl_4$ (70 °C for 30 min), rinsed with EtOH and heated at 500 °C for 30 min. After cooling down to 80 °C the TiO_2 coated plates were immersed into a 0.2 mM solution of the dye for 20 h at room temperature in the dark.

Counter electrodes were prepared according to the following procedure: a 1-mm hole was made in a FTO plate, using diamond drill bits. The electrodes were then cleaned with a detergent solution for 15 min using an ultrasonic bath, 10% HCl, and finally acetone for 15 min using an ultrasonic bath. After thermal treatment at 500 °C for 30 min, 15 μL of a 5 mM solution of H_2PtCl_6 in EtOH was added and the thermal treatment at 500 °C for 30 min repeated. The dye adsorbed TiO_2 electrode and Pt-counter electrode were assembled into a sealed sandwich-type cell by heating with a hot-melt ionomer-class resin (Surlyn 30-μm thickness) as a spacer between the electrodes. A drop of the electrolyte solution was added to the hole and introduced inside the cell by vacuum backfilling. Finally, the hole was sealed with a sheet of Surlyn and a cover glass. A reflective foil at the back side of the counter electrode was taped to reflect unabsorbed light back to the photoanode.

Photovoltaic and photoelectrical characterization of DSSCs: Photovoltaic measurements of DSSCs were carried out under a 500 W Xenon light source (ABET Technologies Sun 2000 class ABA Solar Simulator). The power of the simulated light was calibrated to AM 1.5 (1000 W m^{-2}) using a reference Si cell photodiode equipped with an IR-cutoff filter (KG-5, Schott) to reduce the mismatch in the region of 350–750 nm between the simulated light and the AM 1.5 spectrum. The measurement was repeated with or without a black mask of 0.38 cm^2 surface area placed on top of the photoanode. I—V curves were obtained by applying an external bias to the cell and measuring the generated photocurrent with a Keithley model 2400 digital source meter.

Preparation and characterization of Pt/TiO$_2$ nanopowders: Pt/TiO_2 photocatalyst was prepared by photodeposition of Pt nanoparticles on the surface of TiO_2. Briefly, TiO_2 Degussa P25 (2.0 g) was suspended in a solution of H_2O/EtOH (400 mL) containing 32.7 mg of $Pt(NO_3)_2$, in order to reach a final metal loading of 1.0 wt%. After stirring for 1 h in the dark, the suspension was irradiated with a 450 W medium pressure lamp for 4 h. The material was recovered through centrifugation, washed with EtOH 3 times, and dried under vacuum at 50 °C overnight. The structural properties of the catalyst were checked by XRD (Philips X'Pert diffractometer using a Cu Kα ($\lambda = 0.154$ nm) X-ray source) while the textural properties of the catalyst have been analyzed by N_2 physisorption at the liquid nitrogen temperature (Micromeritics ASAP 2020 automatic analyzer) after degassing the sample under vacuum at 200 °C overnight. Size of Pt nanoparticles was checked by HAADF-STEM (JEOL2010-FEG microscope operating at the acceleration voltage of 200 kV). All the results from characterization are in perfect agreement with previous results.[25c]

Adsorption of dyes on Pt/TiO$_2$: Dye staining was done by suspending 200 mg of Pt/TiO_2 nanopowders in 20 mL of dye solution (0.1 mM in ethanol) for 12 h in the dark. Then the dye@TiO2/Pt nanocomposite was collected by centrifugation, washed twice with ethanol, and dried under vacuum at room temperature overnight. The concentration of the dyes in the supernatant liquid was measured by UV-Vis spectroscopy, confirming the quantitative loading of dyes on the Pt/TiO_2 material.

Hydrogen production through water splitting: The dye-functionalized Pt/TiO_2 nanomaterials have been tested for H_2 production following the optimised procedure described in previous papers.[11a,f,25a–c] Notably, the amount of catalyst has been optimized following the indications recently presented by Kisch and Bahnenmann.[41] 60 mg of the dye@TiO$_2$/Pt catalyst was suspended in 60 mL of 10% v/v aqueous solution of triethanolamine (TEOA) previously neutralized with HCl. After purging with Ar (15 mL min^{-1}) for 30 min, the suspension was irradiated using a 150 W Xe lamp with a cut-off filter at 420 nm. Irradiance was ~6×10^{-3} W m^{-2} in the UV—A range and ~1080 W m^{-2} in the visible range (400–1000 nm). The concentration of H_2 in the gas stream coming from the reactor has been quantified using an Agilent 7890 gaschromatograph equipped with a TCD detector, connected to a Carboxen 1010 column (Supelco, 30 m×0.53 mm ID, 30 μm film) using Ar as carrier.

The performances of the dye-sensitized photocatalysts have been reported in terms of H_2 production rate and overall H_2 productivity. Turn-Over Numbers (TON) were calculated as (2×overall H_2 amount)/(dye loading). Light-to-Fuel Efficiency (LFE) was calculated as [Eq. (1)]:

$$LFE = \frac{F_{H_2} * \Delta H^0_{H_2}}{S * A_{irr}} \tag{1}$$

where F_{H2} is the flow of H_2 produced (expressed in mol s^{-1}), ΔH^0_{H2} is the enthalpy associated with H_2 combustion (285.8 kJ mol^{-1}), S is the total incident light irradiance, as measured by adequate radiometers in 400–1000 nm ranges (expressed in W cm^{-2}) and A_{irr} is the irradiated area (expressed in cm^2).

Dye desorption measurements of sensitized TiO$_2$ films: Dye desorption rate from sensitized TiO_2 films has been investigated by means of optical absorption measurements after specific desorption times, up to 20 min. Commercially available transparent TiO_2 coated glass electrodes have been used for desorption studies (Dyesol MS001630). Electrodes heated at 70 °C have been dipped in 2×10^{-4} M dye solutions in EtOH and left overnight in the dark. They have been rinsed with EtOH and dried under N_2 flux. Each electrode has been dipped in 10 mL of a basic solution of 0.1 M KOH in EtOH/H_2O 15:1 for the required time (2, 4, 7, 10, 15 and 20 minutes) then rinsed with ethanol and dried. UV/Vis transmittance spectra have been measured with a Shimadzu UV-2600 spectrophotometer using the integrating sphere apparatus. The spectra collected before irradiation (t = 0 h) were used as reference data. Degradation data have been reported as relative residual absorbances $A_{max}(t)/A_{max}(0)$, where $A_{max}(t)$ and $A_{max}(0)$ are the absorbances of the dye-sensitized TiO_2 film recorded at their Vis absorption peaks after and before desorption, respectively.

Synthetic procedures

3,3′-(10-octyl-10H-phenothiazine-3,7-diyl)bis (2-cyano-N-((tetrahydro-2H-pyran-2-yl)oxy)acrylamide) (1): N-Methylmorpholine (NMM, 46 mg, 0.45 mmol) and 4-(4,6-Dimethoxy-1,3,5-triazin-2-yl)-4-methylmorpholinium chloride (DMTMM, 100 mg, 0.36 mmol) were added to a solution of **PTZ1** (75 mg, 0.15 mmol) in 20 mL of THF. After 1 h under magnetic stirring at rt the solution colour had become darker than that at the beginning of the experiment. The progress of the reaction has been monitored using TLC. O-(Tetrahydro-2H-pyran-2-yl)hydroxylamine (H_2N-OTHP, 87 mg, 0.75 mmol) was added and the solution recovered the starting colour. After 3 h under magnetic stirring at rt, THF was evaporated and water was added to the mixture, extractions with AcOEt (2×30 mL) were performed and then the combined organic phases were washed with HCl 1 M and water, dried with Na_2SO_4 and filtered. Concentration of the solvent gave the crude product, that was purified through flash column chromatography on silica gel using a mixture of CH_2Cl_2:AcOEt-7:1 as eluent. The desired product has been isolated in 50% yield (53 mg). ^{1}H NMR (400 MHz, CDCl$_3$) δ

EurJOC
European Journal of Organic Chemistry

Research Article
doi.org/10.1002/ejoc.202300924

Chemistry Europe
European Chemical Societies Publishing

9.00 (br s, 2H), 8.13 (s, 2H), 7.80 (dd, $J=8.6$, 2.1 Hz, 2H), 7.59 (t, $J=$ 2.2 Hz, 2H), 6.89 (d, $J=8.7$ Hz, 2H), 5.10–5.04 (m, 2H), 4.06–3.97 (m, 2H), 3.92–3.85 (m, 2H), 3.76–3.64 (m, 2H), 1.98–1.72 (m, 6H), 1.72–1.50 (m, 8H), 1.40–1.14 (m, 10H), 0.93–0.81 (m, 3H). ^{13}C NMR (101 MHz, CDCl$_3$) δ 151.7, 147.5, 131.3, 129.9, 127.2, 124.1, 116.6, 115.7, 103.1, 98.4, 62.9, 48.6, 31.8, 29.9, 29.32, 29.25, 28.1, 26.9, 26.8, 25.1, 22.7, 18.6, 14.2. ESI-MS: m/z 698.74 (100%) [M−1]$^-$.

3,3′-(10-octyl-10H-phenothiazine-3,7-diyl) bis(2-cyano-N-hydroxyacrylamide) (PTZ1-HA): 3,3′-(10-octyl-10H-phenothiazine-3,7-diyl)bis(2-cyano-N-((tetrahydro-2H-pyran-2- yl)oxy)acrylamide) **1** (70 mg, 0.1 mmol) was solubilized in THF and a mixture of water and acetic acid was then added (overall ratio THF:H$_2$O:AcOH– 7:2:1). The mixture was heated to 60 °C for 24 h, protecting it from light using an Al foil. The solvents mixture was then evaporated. The recovered red solid was washed with H$_2$O, petroleum ether, Et$_2$O, and AcOEt, affording the desired product in 85% yield. ^{1}H NMR (400 MHz, THF-$d8$) δ ^{1}H NMR (400 MHz, THF-$d8$) δ 8.06 (s, 2H), 7.89 (dd, $J=8.5$, 1.4 Hz, 2H), 7.73 (d, $J=1.8$ Hz, 2H), 7.10 (d, $J=$ 8.8 Hz, 2H), 4.01 (t, $J=7.0$ Hz, 2H), 1.88–1.78 (m, 2H), 1.53–1.44 (m, 2H), 1.40–1.24 (m, 8H), 0.87 (t, $J=6.8$ Hz, 3H). ^{13}C NMR (101 MHz, THF-$d8$) δ 147.7, 131.1, 129.9, 128.4, 124.4, 116.5 (×2), 100.9, 48.5, 32.5, 30.0, 29.9, 27.3, 25.6, 23.3, 14.2. ESI-MS: m/z 530.31 (100%) [M1]$^-$.

Conflict of Interests

The authors declare no conflict of interest.

Data Availability Statement

The data that support the findings of this study are available from the corresponding author upon reasonable request.

Keywords: DSSC · dye · hydrogen · hydroxamic acid · photocatalysis

[1] C. Zou, Q. Zhao, G. Zhang, B. Xiong, *Nat. Gas Ind. B.* **2016**, *3*, 1–11.
[2] N. Armaroli, V. Balzani, *Angew. Chem. Int. Ed.* **2007**, *46*, 52–66.
[3] a) N. Armaroli, V. Balzani, *Energy for a Sustainable World: From the Oil Age to a Sun-Powered Future*, Wiley-VCH Verlag GmbH & Co. KGaA, Weinheim, **2010**; b) N. Armaroli, V. Balzani, *Chem. Eur. J.* **2016**, *22*, 32–57.
[4] C. Acar, Y. Bicer, M. E. Demir, I. Dincer, *Int. J. Hydrogen Energy* **2019**, *44*, 25347–25364.
[5] J. Barber, P. D. Tran, *J. R. Soc. Interface.* **2013**, *10*, 20120984.
[6] S. Berardi, S. Drouet, L. Francàs, C. Gimbert-Suriñach, M. Guttentag, C. Richmond, T. Stoll, A. Llobet, *Chem. Soc. Rev.* **2014**, *43*, 7501–7519.
[7] K. C. Christoforidis, P. Fornasiero, *ChemCatChem.* **2017**, *9*, 1523–1544.
[8] Z. Wang, C. Li, K. Domen, *Chem. Soc. Rev.* **2019**, *48*, 2109–2125.
[9] a) B. Cecconi, N. Manfredi, T. Montini, P. Fornasiero, A. Abbotto, *Eur. J. Org. Chem.* **2016**, *2016*, 5194–5215; b) C. Decavoli, C. L. Boldrini, F. Faroldi, L. Baldini, F. Sansone, A. Ranaudo, C. Greco, U. Cosentino, G. Moro, N. Manfredi, A. Abbotto, *Eur. J. Org. Chem.* **2022**, *2022*, 145–155; c) M. Watanabe, *Sci. Technol. Adv. Mater.* **2017**, *18*, 705–723; d) G. Reginato, L. Zani, M. Calamante, A. Mordini, A. Dessì, *Eur. J. Inorg. Chem.* **2020**, *2020*, 899–917; e) L. Zani, M. Melchionna, T. Montini, P. Fornasiero, *JPhys Energy* **2021**, *3*, 031001.
[10] A. Hagfeldt, G. Boschloo, L. Sun, L. Kloo, H. Pettersson, *Chem. Rev.* **2010**, *110*, 6595–6663.
[11] a) N. Manfredi, C. Decavoli, C. L. Boldrini, T. H. Dolla, F. Faroldi, F. Sansone, T. Montini, L. Baldini, P. Fornasiero, A. Abbotto, *Eur. J. Org. Chem.* **2021**, *2021*, 284–288; b) J.-F. Huang, Y. Lei, T. Luo, J.-M. Liu, *ChemSusChem.* **2020**, *13*, 5863–5895; c) A. Dessì, M. Monai, M. Bessi, T. Montini, M. Calamante, A. Mordini, G. Reginato, C. Trono, P. Fornasiero, L. Zani, *ChemSusChem.* **2018**, *11*, 793–805; d) O. Bettucci, T. Skaltsas, M. Calamante, A. Dessì, M. Bartolini, A. Sinicropi, J. Filippi, G. Reginato, A. Mordini, P. Fornasiero, L. Zani, *ACS Appl. Energy Mater* **2019**, *2*, 5600–5612; e) M. Bartolini, V. Gombac, A. Sinicropi, G. Reginato, A. Dessì, A. Mordini, J. Filippi, T. Montini, M. Calamante, P. Fornasiero, L. Zani, *ACS Appl. Energy Mater* **2020**, *3*, 8912–8928; f) N. Manfredi, M. Monai, T. Montini, M. Salamone, R. Ruffo, P. Fornasiero, A. Abbotto, *Sustain. Energy Fuels* **2017**, *1*, 694–698.
[12] a) Y. Geng, C. Yi, M. P. Bircher, S. Decurtins, M. Cascella, M. Grätzel, S.-X. Liu, *RSC Adv.* **2015**, *5*, 98643–98652; b) S. Liu, Y. Jiao, Y. Ding, X. Fan, J. Song, B. Mi, Z. Gao, *Dyes Pigm.* **2020**, *180*, 108470; c) J. Warnan, J. Willkomm, Y. Farré, Y. Pellegrin, M. Boujtita, F. Odobel, E. Reisner, *Chem. Sci.* **2019**, *10*, 2758–2766.
[13] W. Lee, S. B. Yuk, J. Choi, H. J. Kim, H. W. Kim, S. H. Kim, B. Kim, M. J. Ko, J. P. Kim, *Dyes Pigm.* **2014**, *102*, 13–21.
[14] a) R. Harikisun, H. Desilvestro, *Sol. Energy* **2011**, *85*, 1179–1188; b) L. Zhang, J. M. Cole, *ACS Appl. Mater. Interfaces* **2015**, *7*, 3427–3455.
[15] a) Y. Zhang, C.-R. Zhang, W. Wang, J.-J. Gong, Z.-J. Liu, H.-S. Chen, *Comput. Theor. Chem.* **2016**, *1095*, 125–133; b) K. L. Materna, R. H. Crabtree, G. W. Brudvig, *Chem. Soc. Rev.* **2017**, *46*, 6099–6110.
[16] E. Bae, W. Choi, J. Park, H. S. Shin, S. B. Kim, J. S. Lee, *J. Phys. Chem. B.* **2004**, *108*, 14093–14101.
[17] A. Baktash, B. Khoshnevisan, A. Sasani, K. Mirabbaszadeh, *Org. Electron.* **2016**, *33*, 207–212.
[18] D. G. Brown, P. A. Schauer, J. Borau-Garcia, B. R. Fancy, C. P. Berlinguette, *J. Am. Chem. Soc.* **2013**, *135*, 1692–1695.
[19] K. Ladomenou, T. N. Kitsopoulos, G. D. Sharma, A. G. Coutsolelos, *RSC Adv.* **2014**, *4*, 21379–21404.
[20] P. Kumaresan, S. Vegiraju, Y. Ezhumalai, S. L. Yau, C. Kim, W.-H. Lee, M.-C. Chen, *Polymer* **2014**, *6*, 2645–2669.
[21] S. Thogiti, S. Vuppala, H. L. Cha, N. T. Thuong Thuong, H. J. Jo, R. K. Chitumalla, S. C. Hee, C. T. Thanh Thuy, J. Jang, J. H. Jung, G. Koyyada, J. H. Kim, *J. Photochem. Photobiol. A.* **2020**, *398*, 112512.
[22] W. R. McNamara, R. C. Snoeberger Iii, G. Li, C. Richter, L. J. Allen, R. L. Milot, C. A. Schmuttenmaer, R. H. Crabtree, G. W. Brudvig, V. S. Batista, *Energy Environ. Sci.* **2009**, *2*, 1173–1175.
[23] F. Ambrosio, N. Martsinovich, A. Troisi, *J. Phys. Chem. Lett.* **2012**, *3*, 1531–1535.
[24] a) C. Koenigsmann, T. S. Ripolles, B. J. Brennan, C. F. Negre, M. Koepf, A. C. Durrell, R. L. Milot, J. A. Torre, R. H. Crabtree, V. S. Batista, G. W. Brudvig, J. Bisquert, C. A. Schmuttenmaer, *Phys. Chem. Chem. Phys.* **2014**, *16*, 16629–16641; b) W. R. McNamara, R. L. Milot, H.-E. Song, R. C. Snoeberger Iii, V. S. Batista, C. A. Schmuttenmaer, G. W. Brudvig, R. H. Crabtree, *Energy Environ. Sci.* **2010**, *3*, 917–923; c) T. Higashino, Y. Kurumisawa, N. Cai, Y. Fujimori, Y. Tsuji, S. Nimura, D. M. Packwood, J. Park, H. Imahori, *ChemSusChem.* **2017**, *10*, 3347–3351.
[25] a) N. Manfredi, M. Monai, T. Montini, F. Peri, F. De Angelis, P. Fornasiero, A. Abbotto, *ACS Energy Lett.* **2017**, *3*, 85–91; b) N. Manfredi, B. Cecconi, V. Calabrese, A. Minotti, F. Peri, R. Ruffo, M. Monai, I. Romero-Ocana, T. Montini, P. Fornasiero, A. Abbotto, *Chem. Commun.* **2016**, *52*, 6977–6980; c) B. Cecconi, N. Manfredi, R. Ruffo, T. Montini, I. Romero-Ocaña, P. Fornasiero, A. Abbotto, *ChemSusChem.* **2015**, *8*, 4216–4228; d) P. S. Gangadhar, G. Reddy, S. Prasanthkumar, L. Giribabu, *Phys. Chem. Chem. Phys.* **2021**, *23*, 14969–14996.

[26] B. Cecconi, *Artificial Photosynthesis: Molecular Approaches for Photocatalytic Hydrogen Production, PhD Thesis*, University of Milano-Bicocca, **2016**, https://hdl.handle.net/10281/100472.

[27] a) A. S. Reddy, M. S. Kumar, G. R. Reddy, *Tetrahedron Lett.* **2000**, *41*, 6285–6288; b) A. A. Zur, H.-C. Chien, E. Augustyn, A. Flint, N. Heeren, K. Finke, C. Hernandez, L. Hansen, S. Miller, L. Lin, *Bioorg. Med. Chem. Lett.* **2016**, *26*, 5000–5006.

[28] a) B. Kolesińska, K. Kasperowicz, M. Sochacki, A. Mazur, S. Jankowski, Z. J. Kamiński, *Tetrahedron Lett.* **2010**, *51*, 20–22; b) P. P. Z. J. Kamiński, J. Rudziński, *J. Org. Chem.* **1998**, *63*, 4248–4425.

[29] a) Z. J. Kamiński, B. Kolesińska, J. Kolesińska, G. Sabatino, M. Chelli, P. Rovero, M. Błaszczyk, M. L. Główka, A. M. Papini, *J. Am. Chem. Soc.* **2005**, *127*, 16912–16920; b) L. Banach, L. Janczewski, J. Kajdanek, K. Milowska, J. Kolodziejczyk-Czepas, G. Galita, W. Rozpedek-Kaminska, E. Kucharska, I. Majsterek, B. Kolesinska, *Molecules* **2022**, *27*, 2271; c) J. P. Z. J. Kaminki, *Chem.* **1990**, *332* 579–583.

[30] a) G. Moroy, C. Denhez, H. El Mourabit, A. Toribio, A. Dassonville, M. Decarme, J.-H. Renault, C. Mirand, G. Bellon, J. Sapi, A. J. P. Alix, W. Hornebeck, E. Bourguet, *Bioorg. Med. Chem.* **2007**, *15*, 4753–4766; b) K. Kumar, R. Das, B. Thapa, B. Rakhecha, S. Srivastava, K. Savita, M. Israr, D. Chanda, D. Banerjee, K. Shanker, D. U. Bawankule, B. Santini, M. L. Di Paolo, L. D. Via, D. Passarella, A. S. Negi, *Bioorg. Med. Chem.* **2023**, *86*, 117300.

[31] K. Kalyanasundaram, *Dye-Sensitized Solar Cells*, EPFL Press, New York, **2010**, pp. 49–52.

[32] C. Barolo, M. K. Nazeeruddin, S. Fantacci, D. Di Censo, P. Comte, P. Liska, G. Viscardi, P. Quagliotto, F. De Angelis, S. Ito, M. Grätzel, *Inorg. Chem.* **2006**, *45*, 4642–4653.

[33] a) N. P. Liyanage, A. Yella, M. Nazeeruddin, M. Grätzel, J. H. Delcamp, *ACS Appl. Mater. Interfaces* **2016**, *8*, 5376–5384; b) P. Brogdon, H. Cheema, J. H. Delcamp, *ChemSusChem.* **2018**, *11*, 86–103.

[34] J. O. M. Bockris, S. U. M. Khan, *Surface Electrochemistry-A Molecular Level Approach*, Springer US, New York, **1993**.

[35] T. P. Brewster, S. J. Konezny, S. W. Sheehan, L. A. Martini, C. A. Schmuttenmaer, V. S. Batista, R. H. Crabtree, *Inorg. Chem.* **2013**, *52*, 6752–6764.

[36] a) D. Mahanta, G. Madras, S. Radhakrishnan, S. Patil, *J. Phys. Chem. B.* **2009**, *113*, 2293–2299; b) H.-J. Son, C. Prasittichai, J. E. Mondloch, L. Luo, J. Wu, D. W. Kim, O. K. Farha, J. T. Hupp, *J. Am. Chem. Soc.* **2013**, *135*, 11529–11532.

[37] a) B. Cecconi, A. Mordini, G. Reginato, L. Zani, M. Taddei, F. Fabrizi de Biani, F. D. Angelis, G. Marotta, P. Salvatori, M. Calamante, *Asian J. Org. Chem.* **2014**, *3*, 140–152; b) D. Franchi, M. Calamante, G. Reginato, L. Zani, M. Peruzzini, M. Taddei, F. Fabrizi de Biani, R. Basosi, A. Sinicropi, D. Colonna, A. Di Carlo, A. Mordini, *Tetrahedron* **2014**, *70*, 6285–6295.

[38] a) S. Cao, L. Piao, *Angew. Chem. Int. Ed.* **2020**, *59*, 18312–18320; b) Z. Wang, T. Hisatomi, R. Li, K. Sayama, G. Liu, K. Domen, C. Li, L. Wang, *Joule* **2021**, *5*, 344–359.

[39] D. F. Shriver, M. A. Dreazdon, *The Manipulation of Air-Sensitive Compounds*, John Wiley & Sons, New York, **1986**.

[40] S. Ito, T. N. Murakami, P. Comte, P. Liska, C. Grätzel, M. K. Nazeeruddin, M. Grätzel, *Thin Solid Films* **2008**, *516*, 4613–4619.

[41] H. Kisch, D. Bahnemann, *J. Phys. Chem. Lett.* **2015**, *6*, 1907–1910.